Journal of Magnetism and Magnetic Materials 475 (2019) 533–538

Contents lists available at ScienceDirect

Journal of Magnetism and Magnetic Materials

journal homepage: www.elsevier.com/locate/jmmm

Research articles

Development of an optical pumped gradiometric system to detect magnetic relaxation of magnetic nanoparticles

O. Baffa[a,*], R.H. Matsuda[a], S. Arsalani[a], A. Prospero[b], J.R.A. Miranda[b], R.T. Wakai[c]

[a] Departamento de Física, FFCLRP, USP, Ribeirão Preto, SP, Brazil
[b] Departamento de Física e Biofísica, Instituto de Biociências, UNESP, Botucatu, SP, Brazil
[c] Department of Medical Physics, University of Wisconsin-Madison, Madison, WI, USA

A B S T R A C T

The investigation of magnetic nanoparticles for medical and biological applications is relatively recent and steadily growing. When properly functionalized, magnetic nanoparticles (MNPs) can target cancer cells and deliver a drug or heat to these cells. MNPs are being investigated in several applications in medicine such as hyperthermia, magnetic particle imaging, cell separation and magnetofection, *in vitro* and *in vivo* alternating current biosusceptibility, T1 and T2 magnetic resonance contrast agents, and magnetorelaxometry. In each of these applications, a specific physical property is measured. Magnetorelaxometry relies on the fact that when MNPs are magnetized they can relax by the Brownian and Néel mechanisms. Both mechanisms depend on the MNP size and for certain conditions can have a faster relaxation through the Brownian, compared to the Néel, mechanism. This can be exploited to target cells. For certain sizes, when an MNP is free to rotate in the biological fluids, they will relax faster than when attached to a cell. This can provide a high contrast for detection of magnetically-labelled cancer cells, making it possible to differentiate normal from cancer tissue. Until very recently SQUIDs were the main detectors employed to measure MNPs, but Optically Pumped Magnetometers (OPM) are now an attractive alternative. OPMs are smaller, do not need liquid helium, and are simpler to operate than SQUIDs. Here, we present the initial steps of the development of an OPM-based instrument to measure relaxation of MNP *in vitro*.

1. Introduction

Over the last few decades, magnetic nanoparticles (MNPs) have proven to be a major advance in several areas of biomedical and clinical research [1,2]. Due to their intrinsic properties, it is possible to characterize and monitor these materials using magnetic fields and magnetic field detectors. In order to increase the applicability of MNPs, several magnetic techniques have been developed and applied, such as magnetic particle imaging (MPI) [3,4], magnetic resonance imaging (MRI) [5,6], AC biosusceptometry [7–10], fluxgate [11,12] and superconducting quantum interference device (SQUID) [13–15]. Each of these techniques relies on one or more specific physical properties of the MNPs. The MPI system takes advantage of the fact that the MNPs have a nonlinear magnetization behavior, which provides harmonic signals that can be used to track the particles *in vivo*. MRI can use the particles as T1 and T2 contrast agents, where the MNPs change the proton relaxation of the tissue around them. AC biosusceptometry exploits the MNPs magnetic susceptibility to determine the fate of the particles in both *ex vivo* and *in vivo* situations. Fluxgates and SQUIDs have been used to detect the magnetization of MNPs after a brief exposure to a magnetizing field. Due to their high sensitivity and accuracy, SQUIDs have been employed in several MNPs studies for both *in vitro* and *in vivo* models and have been the most widely used detectors for magnetorelaxometry (MRX) studies [16,17].

MRX detects the time dependent relaxation of MNPs by Brownian and Néel mechanisms, after a brief magnetization pulse [17,18]. Brownian relaxation relies on the physical rotation of the nanoparticle in the fluid medium, whereas Néel relaxation is based on the direction change of the magnetic moment relative to the crystal orientation. Both mechanisms depend on the MNP size and, for certain sizes, one can have a faster relaxation by Brownian when compared to Néel mechanism. Thus, this property can be applied to study MNP characteristics [19–21], their environment [22], immunoassays [23–25], specific cells and tissues labeled by MNPs [26], and, most recently, to perform MNP biodistribution imaging *in vivo* [14,27]. There are also other possibilities under investigation that can be combined with MRX, such as magnetic hyperthermia, drug delivery, cell separation, MRI, and MPI studies.

Various experimental techniques have been used for MRX studies. Fluxgate detectors [12,28] were used initially, but since the early 90′s SQUIDs are the main detectors employed. Improvements have been made to increase the SQUIDs performance in systems dedicated to MRX. Matz and co-workers developed a SQUID system with improved geometry and electronics for MRX immunoassays [24]. In order to observe the Brownian relaxation in the time domain, Haller and co-workers used coupled read-out electronics and a flux-locked loop to

* Corresponding author.
E-mail address: baffa@usp.br (O. Baffa).

https://doi.org/10.1016/j.jmmm.2018.10.067
Received 23 June 2018; Received in revised form 10 September 2018; Accepted 13 October 2018
Available online 15 October 2018
0304-8853/

decrease the SQUID dead time after the magnetizing pulse [29]. Other improvements for specific applications were made, such as the use of integrated planar LTS-SQUID gradiometers to allow the study of larger objects in disturbed environments [30] and the adaptation of an magnetoencephalography SQUID system for *in vivo* MRX [31].

Recently, a new class of high sensitivity magnetometers has been developed and utilized for MRX studies [16]. Atomic magnetometers, also known as optically pumped magnetometers (OPMs), have seen major improvements in the past few years [32]. OPM sensors with chip-scale dimensions were developed by the National Institute of Standards and Technology (NIST) and have demonstrated sensitivities below 200 $fT/Hz^{1/2}$ [32]. These magnetometers have been applied to fetal magnetocardiography [33,34] and magnetoencephalography studies [35,36]. This new class of atomic magnetometers have significant advantages over SQUID systems. These include lower-power operation, cryogen-free operation, low-cost manufacturing, smaller dimensions, and closer proximity to the magnetic field source [32].

Here we describe the construction of an instrument to be used for MRX *in vitro* studies. To build the system we employed two off-the-shelf OPM sensors (QuSpin Inc., Louisville, Colorado, USA) and a small magnetically-shielded cylindrical chamber. The use of two sensors allows the subtraction of the residual environmental noise from a reference signal in order to increase the signal-to-noise ratio. The dimensions of the experimental setup allow the entire system to be small and portable, which can help MRX immunoassays achieve widespread use.

2. Materials and methods

2.1. Description of the set up

Two OPMs were assembled in an axial configuration and were oriented in opposite directions. The one closest to the sample was called the master sensor and other was called the slave sensor. A 3D printed plastic holder was produced so that the OPMs could be inserted into rectangular openings at the end. In the central region between them, a sample holder was placed together with a pair of circular coils. A small slanted opening on the left side of the holder (Fig. 1A) allowed insertion of the sample close to the OPM at the right of the holder. A flexible plastic tube served as a guide for the sample that was pushed from the outside through a flexible PVC rod with a sample chamber at the end. The whole set up was placed inside a small, cylindrical magnetically-shield enclosure (Zero Gauss Chamber, Magnetic Shield Corporation, ZG 206) with internal diameter of 152 mm, inside depth 381 mm, outside diameter 210 mm. The shield incorporated 3 layers of high permeability material with thickness 0.64 mm, producing an attenuation factor for static fields of about 1,500. Since the local earth's field is 20 μT this shielding gives a residual magnetic field inside the chamber of around 10 nT. The plastic tube guide and sample holder allowed easy sample changes without having to open the chamber every time a new sample was studied. The samples were inserted in hematocrit glass tubes having 1 mm internal diameter. Some samples were in the liquid state and others were immobilized by absorption onto a paper filter. The tubes were sealed at one end using dental mold wax and at the other by heat.

The OPMs used in this work are magnetometers. Samples were placed in the sample holder and positioned inside the system. Magnetic pulses were applied, and the relaxation signal was acquired in both OPMs. All signals were acquired and low-pass filtered by the OPM electronics with 150 Hz cut-off frequency. Following the signal recording, an off-line gradiometer software was designed to subtract one OPM signal from the other.

2.2. Magnetizing circuit

Fig. 2 shows the wiring diagram of the circuit used to apply the current pulse to the two five-turn, 1 cm diameter coils. It is powered with a 12 V battery and switched on and off with a relay. The 1 Ω resistor controls the current intensity. A flyback diode prevents the circuit from ringing. The inverting switch allows us to apply pulses with different polarities and can be used to average measurements and cancel any remnant magnetization induced in the sample. The single-pole double-throw switch is used to commute the coils from a simple centered coil to a Helmholtz configuration. The single coil configuration is at equal distance from each OPM and, when excited, the response of the OPMs can be recorded and differences in sensitivities can be accounted for when composing the software gradiometer. With the present set up a magnetizing field pulse of 9 mT amplitude can be applied to the sample.

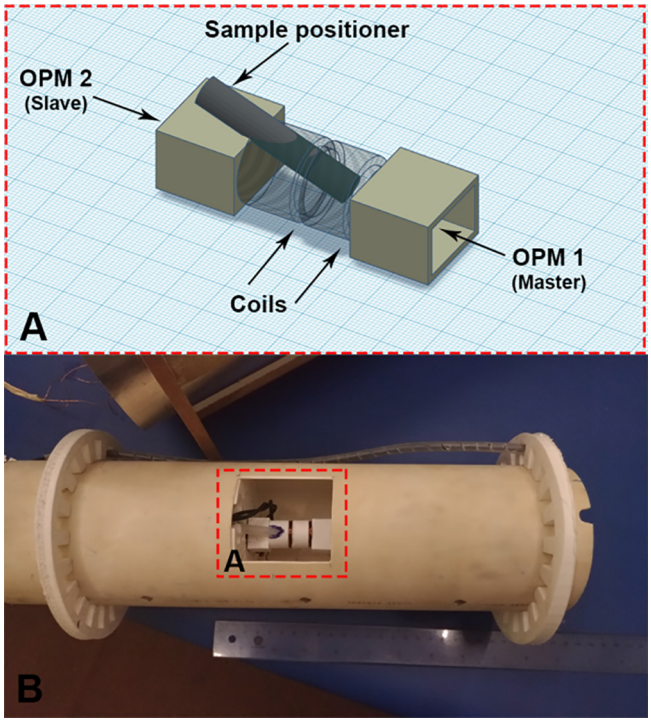

Fig. 1. (a) Schematic of the 3D-printed holder for the OPMs showing the opening to insert the sample. (b) Picture of the complete set up for insertion in the magnetic enclosure, with the magnetizing coils at right, flexible plastic tube to guide the sample into position. The external rims are opened and allows air circulation in the magnetically shielded chamber.

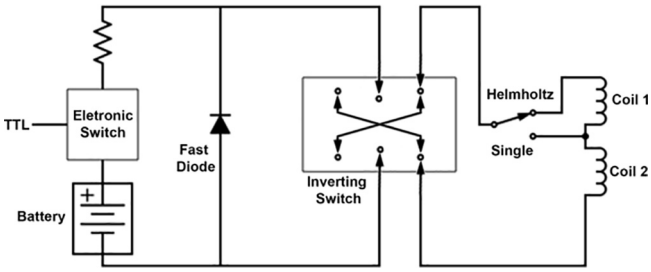

Fig. 2. Circuit diagram for the magnetization of the sample.

2.3. Nanoparticles:

Three different nanoparticle types were used: Chemicell fluidMAG-Chitosan with diameter 2 μm, Precision MRX with diameter 25 nm, and magnetic nanoparticles synthesized in our laboratory.

Magnetic nanoparticles (Fe_3O_4) were synthesized in our laboratory by a simple co-precipitation method at mild temperature. Briefly,

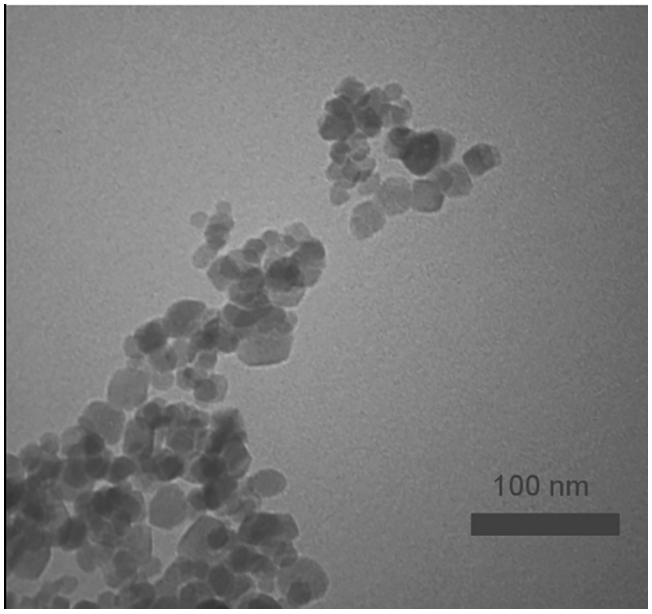

Fig. 3. TEM image of the magnetic nanoparticle synthesized.

0.337 g of iron (III) chloride ($FeCl_3{\cdot}6H_2O$) was dissolved in 12.5 ml distilled water. Then, 0.198 g of iron (II) chloride ($FeCl_2{\cdot}4H_2O$) was dissolved in a 5 ml water solution of hydrochloride acid (2.725 M). Next, the mixture of iron (III) chloride (4 ml) and iron (II) chloride (1 ml) was rapidly added to NH_4OH water solution (1.28 M) at 90 °C with vigorous stirring. The color of the solution changed immediately to black, indicating the formation of magnetite nanoparticles (Fe_3O_4). To prevent agglomeration, magnetic nanoparticles were kept in an ultrasonic bath for one hour. Finally, MNPs were magnetically separated and after 4 times washing with deionized water, MNPs were dried in an oven at 32 °C.

A Transmission Electron Microscopy (TEM) image of MNPs is shown in Fig. 3. It shows that the nanoparticles are nearly spherical.

Fig. 4 shows the x-ray diffraction pattern (XRD) of the MNPs. XRD patterns of the synthesized MNPs reveal diffraction peaks at (1 1 1), (2 2 0), (3 1 1), (4 0 0), (4 2 2), (5 1 1), and (4 4 0) which are the characteristic peaks of the pure magnetite (Fe_3O_4) with a cubic spinel structure (JCPDS database) [37]. The calculation of the size of the

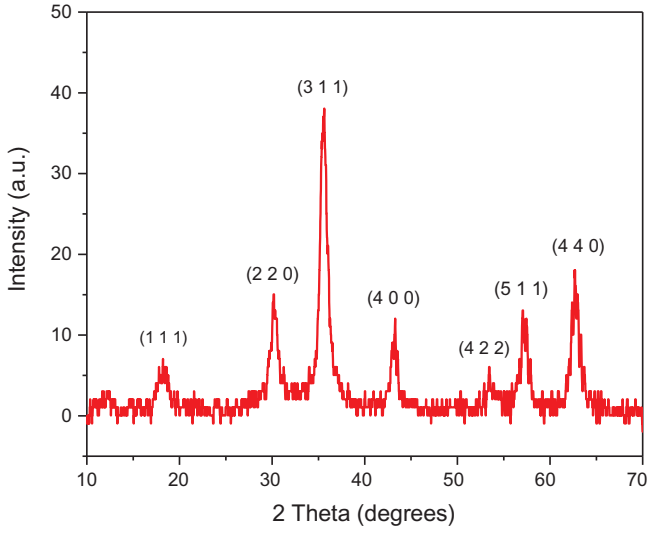

Fig. 4. X-ray diffraction pattern of the magnetic nanoparticle synthesized in our laboratory.

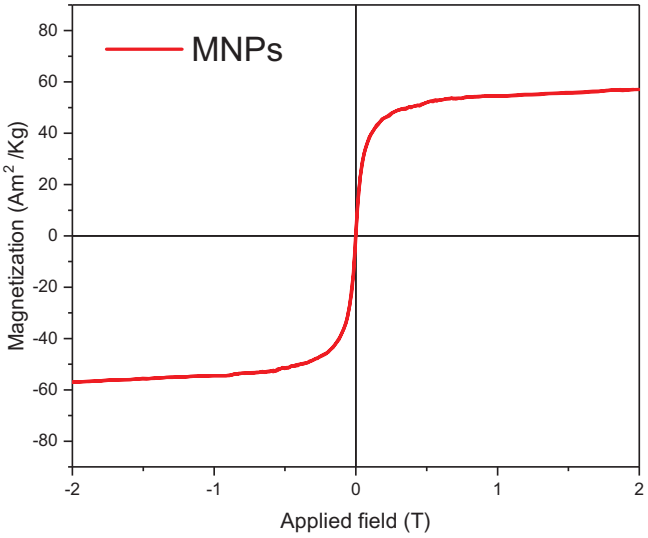

Fig. 5. Magnetization curve of the homemade magnetic nanoparticles measured with a Hall probe magnetometer.

magnetic nanoparticle was carried out using Scherrer's equation. The calculations result showed that the particle size was 9 nm. Transmission scanning microscopy was also performed and confirmed this average diameter. However, these MNPs have a wide diameter distribution, reaching diameters of 25 nm.

Fig. 5 shows the magnetization curve of the magnetic nanoparticles obtained using a Hall probe magnetometer developed by Araujo and coworkers [38]. The data indicates immeasurably small values of coercivity field and remnant magnetization. It shows that the synthesized particles exhibit superparamagnetic properties at room temperature. The saturation magnetization of the nanoparticles was found to be 57 Am^2/kg (emu/g).

2.4. Data analysis

All raw signals were processed using Origin Microcal plotting software. The fitting of experimental transient data is a difficult task. Flynn and Bryant [31] used a complex function containing a DC term, one logarithmic function to account for Neel relaxation, one exponential for Brownian relaxation, and a sinusoidal function for the applied pulse. We decided to try an empirical function containing a constant term and two exponentials:

$$S = a_0 + a_1 e^{\left(\frac{-t}{\tau_1}\right)} + a_2 e^{\left(\frac{-t}{\tau_2}\right)} \quad (1)$$

In this equation, a_0 represents an arbitrary (offset) static field and the other two terms represent the Neel relaxation and the instrumental contribution. This simple model concentrates in the instrumental contribution everything that is not related to MNP relaxation. This is an empirical equation, and to separate each contribution to the instrumental contribution requires designing specific experiments.

The first-order gradiometer software was constructed by following two steps. The first step was to remove the static magnetic field component by subtracting the signal from the baseline before the pulse. The second part was to subtract the slave signal from the master signal. The exponential fit was applied to the resulting signal.

3. Results and discussion

Fig. 6 shows the noise level of the OPMs inside the small shielding enclosure. The noise floor was 30 $fT/(Hz)^{1/2}$. Residual interferences at 60 Hz and other frequencies are also present.

Fig. 7 shows the temporal response of the OPMs. Once the OPMs can

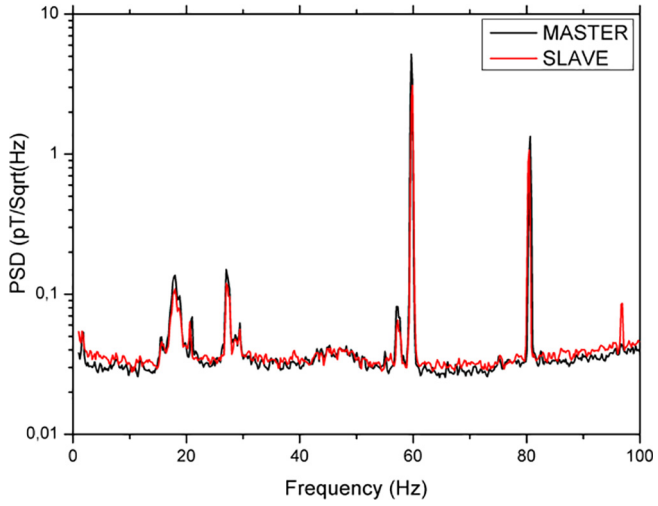

Fig. 6. Noise spectra of the OPMs inside the small magnetic enclosure. A noise floor of 30 fT was obtained with residual fields at 60 Hz and other frequencies.

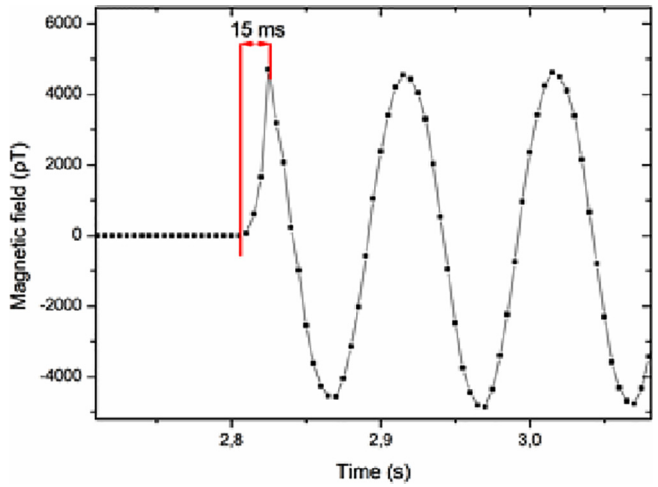

Fig. 7. Magnetic field measured by the OPM produced by an oscillatory signal in the presence of the magnetizing magnetic pulse. The dead time was estimated from the end of the applied pulse and the beginning of the recuperation of the sinusoidal.

saturate with the magnetizing pulses above 5 nT, there is a dead time during which the OPMs recover from the magnetizing pulse and cannot detect the MNP signal. To measure the dead time another coil was placed inside the magnetic shielding and driven with a 10 Hz sinusoidal signal of low amplitude. The dead time was measured from the end of the applied pulse to the beginning of the recuperation of the sinusoidal signal and was estimated to be 15 ms. The applied pulse is strong enough to saturate the OPM sensor, so the signal is zero in the first part of the tracing.

The first-order gradiometer was used to decrease the OPM signal noise. Fig. 8 shows the signals from the master and slave sensors and the resulting first-order gradiometer signal.

The first relaxation measurements performed were done with MNPs in solution. Large MNPs and viscous fluids were used to produce relaxation times τ compatible with the time window of our instrument. When particles are free to move the relaxation is dominated by Brownian motion and we have:

$$\tau_B = \frac{4\eta\pi r^3}{k_B T}$$

where r is the radius of the MNP, η is the viscosity, k_B is the Boltzmann

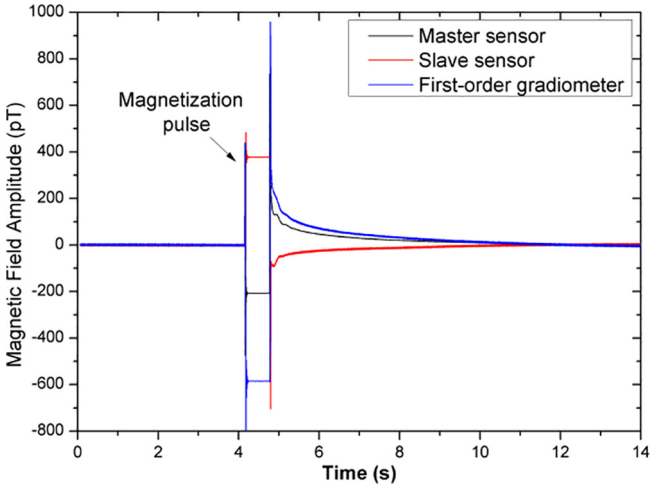

Fig. 8. Master and slave sensors signals and the resulting first-order gradiometer signal. The sample was 4 µl MRX-MNP in solvent.

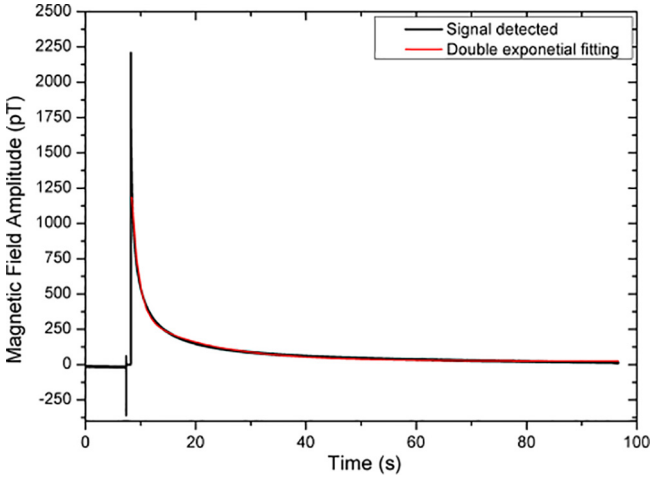

Fig. 9. Representative plot of the signal versus time obtained from for the fluidMAG-Chitosan MNP. The data was fitted to Eq. (1), yielding a_0 = 24pT, a_1 = 361pT, a_2 = 2155pT, τ_1 = 13 s, and τ_2 = 1.26 s. The coefficient of determination, R^2, was 0.995.

constant, and T the temperature.

Fig. 9 shows the measurements obtained with the fluidMAG-Chitosan MNPs with the two OPMs forming an off-line software gradiometer.

Using a time constant of 1.26 s, found by the double exponential fit, and assuming the viscosity is the same as that of water, we get a radius of r = 0.77 µm. A dynamical light scattering (DLS) measurement made immediately after the measurement gave a radius of r = 0.81 µm, in excellent agreement.

In another experiment we used the MRX-MNP and measured the relaxation with the particles in fluid and fixed in paper filter. The results can be seen in Fig. 10. As expected, for the samples dispersed in the liquid the MNPs relaxed rapidly due to Brownian motion and did not give a measurable signal. However, when they were fixed in the paper filter the only way for them to relax would be by Néel relaxation, and a relaxation curve could be measured. The Néel relaxation is given by the following expression:

$$\tau_N = \tau_0 e^{\frac{KV}{kT}}$$

where τ_0 is usually assumed to be 1 ns–0.1 ns, K is the effective anisotropy energy density of the magnetic material and V is the volume of the magnetic particle [39]. Using K = 1.35 10^4 J m^{-3}, T = 300 K, and a

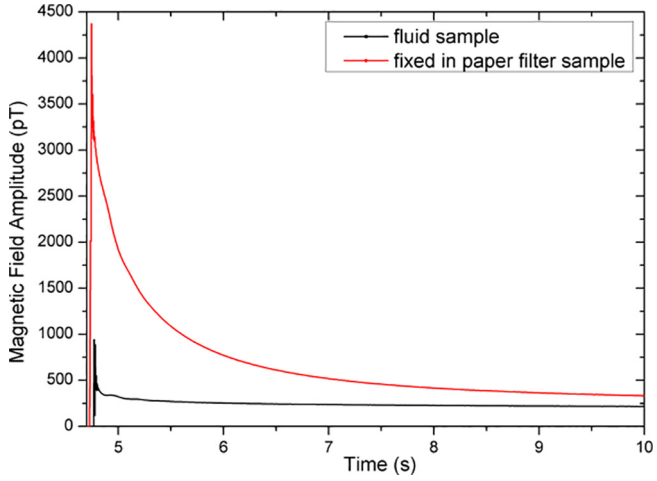

Fig. 10. Representative plot of the signal versus time obtained from for the PrecisionMRX MNP freely to rotate in a fluid and fixed in paper filter. The Neel relaxation can be clearly see with a time constant τ = 1–2 s.

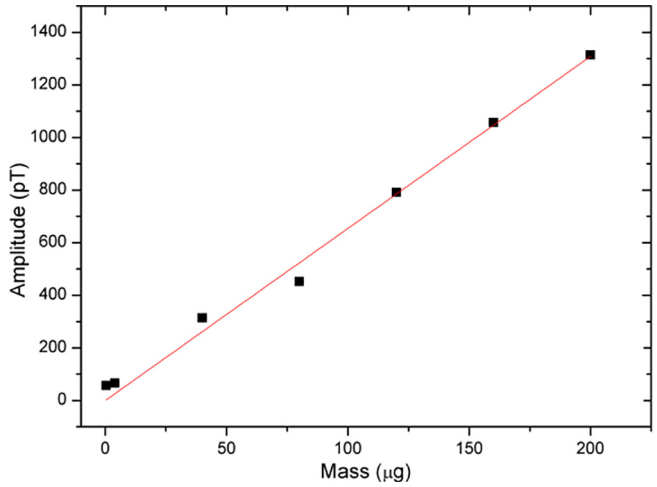

Fig. 11. Calibration plot of the signal versus concentration for the PrecisionMRX MNP fixed in paper filter. The amplitude of the exponential fitting is used as an indication of the signal intensity. The signal intensity is given by the equation $y = 6.54x$, where y is the amplitude in pT and x the mass in μg, with an R^2 = 0.996 and a standard error of ± 0.15 in the slope.

diameter of 25 nm the relaxation times are 1–2 s.

The data show τ = 1–2 s, in good agreement with our expectation for these particles. The original samples were diluted, and measurements were performed to produce a calibration curve of signal intensity versus concentration (Fig. 11).

Finally, we decided to test also the homemade NRL-MNPs. Although they have a wide dispersion of diameters and most will not give a Neel relaxation in the range of time that can be measured by our instrumentation, they can still serve as a useful test of the system. The relaxation curves were similar to those observed for the other samples. The calibration curve is shown in Fig. 12. It can be seen that the amount of mass necessary to produce a detectable MRX signal is about 50 times higher than that needed for the PrecisionMRX MNPs, which have a dispersion of only 1 nm around its mean value of 25 nm.

4. Conclusions

We demonstrated, for the first time, the use of an off-the-shelf OPM magnetometer for MRX studies. The OPM-based system we developed was able to detect relaxation in several different types of MNPs. The

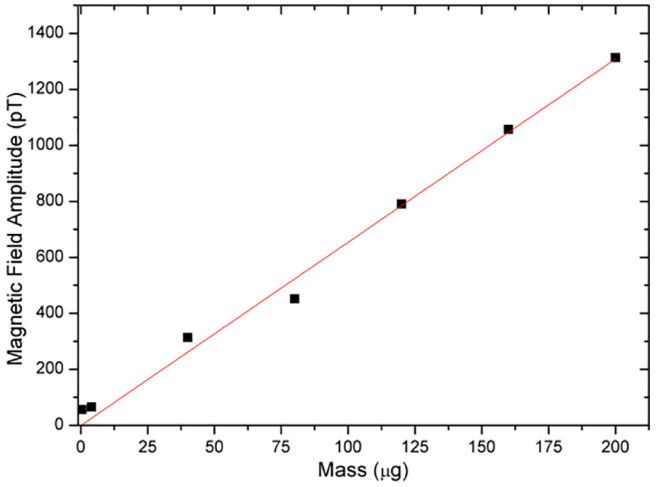

Fig. 12. Calibration plot of the signal versus concentration for the homemade NRL-MNP fixed in paper filter. The amplitude of the exponential fitting is used as an indication of the signal intensity. The coefficient of determination R^2 = 0.994 was obtained.

results showed good agreement with the DLS data. Using the sample positioning rod, we were able to decrease the time between the measurements. The entire system has small dimensions, which improved its portability. In summary, using readily available components we developed a system to perform fast and precise MRX measurements. This can potentially lead to increased use of MXP for research and clinical applications.

Acknowledgements

Partial financial support: FAPESP Grant 2016/06032-0, CNPq (S.A. Scholarship and Grant 407471/2016-2) and CAPES Finance Code 001. To PrecisionMRX- Trailblazers program for the donation of MNPs.

Appendix A. Supplementary data

Supplementary data to this article can be found online at https://doi.org/10.1016/j.jmmm.2018.10.067.

References

[1] Q.A. Pankhurst, N.T.K. Thanh, S.K. Jones, J. Dobson, Progress in applications of magnetic nanoparticles in biomedicine, J. Phys. D Appl. Phys. 42 (2009).
[2] A. Singh, S.K. Sahoo, Magnetic nanoparticles: a novel platform for cancer theranostics, Drug Discovery Today 19 (2014) 474–481.
[3] B. Gleich, J. Weizenecker, Tomographic imaging using the nonlinear response of magnetic particles, Nature 435 (2005) 1214–1217.
[4] J. Weizenecker, B. Gleich, J. Rahmer, H. Dahnke, J. Borgert, Three-dimensional real-time in vivo magnetic particle imaging, Phys. Med. Biol. 54 (2009) L1–L10.
[5] C. Sun, J.S. Lee, M. Zhang, Magnetic nanoparticles in MR imaging and drug delivery, Adv. Drug Deliv. Rev. 60 (2008) 1252–1265.
[6] B. Bonnemain, Superparamagnetic agents in magnetic resonance imaging: physicochemical characteristics and clinical applications. A review, J. Drug Targeting 6 (1998) 167–174.
[7] A.G. Prospero, C.C. Quini, A.F. Bakuzis, P. Fidelis-de-Oliveira, G.M. Moretto, F.P. Mello, M.F. Calabresi, R.V. Matos, E.A. Zandona, N. Zufelato, R.B. Oliveira, J.R. Miranda, Real-time in vivo monitoring of magnetic nanoparticles in the bloodstream by AC biosusceptometry, J. Nanobiotechnol. 15 (2017) 22.
[8] C.C. Quini, A.G. Prospero, M.F.F. Calabresi, G.M. Moretto, N. Zufelato, S. Krishnan, D.R. Pina, R.B. Oliveira, O. Baffa, A.F. Bakuzis, J.R.A. Miranda, Real-time liver uptake and biodistribution of magnetic nanoparticles determined by AC biosusceptometry, Nanomed. Nanotechnol. Biol. Med. 13 (2017) 1519–1529.
[9] C.C. Quini, J.F. Matos, A.G. Próspero, M.F. Calabresi, N. Zufelato, A.F. Bakuzis, O. Baffa, J.R. Miranda, Renal perfusion evaluation by alternating current biosusceptometry of magnetic nanoparticles, J. Magn. Magn. Mater. (2014).
[10] B.W. Ficko, P.M. Nadar, P.J. Hoopes, S.G. Diamond, Development of a magnetic nanoparticle susceptibility magnitude imaging array, Phys. Med. Biol. 59 (2014) 1047.
[11] F. Ludwig, E. Heim, S. Mäuselein, D. Eberbeck, M. Schilling, Magnetorelaxometry of magnetic nanoparticles with fluxgate magnetometers for the analysis of biological

targets, J. Magn. Magn. Mater. 293 (2005) 690–695.
[12] F. Ludwig, E. Heim, D. Menzel, M. Schilling, Investigation of superparamagnetic Fe 3 O 4 nanoparticles by fluxgate magnetorelaxometry for use in magnetic relaxation immunoassays, J. Appl. Phys. 99 (2006) 08P106.
[13] E.H. Ladino, N. Zufelato, A. Bakuzis, A.O. Carneiro, D. Covas, O. Baffa, Detection of magnetic nanoparticles with a large scale AC superconducting susceptometer, Supercond. Sci. Technol. 30 (2017) 084007.
[14] M. Liebl, F. Wiekhorst, D. Eberbeck, P. Radon, D. Gutkelch, D. Baumgarten, U. Steinhoff, L. Trahms, Magnetorelaxometry procedures for quantitative imaging and characterization of magnetic nanoparticles in biomedical applications, Biomed. Eng./Biomedizinische Technik 60 (2015) 427–443.
[15] J.J. Chieh, K.W. Huang, Y.Y. Lee, W.C. Wei, Dual-imaging model of SQUID biosusceptometry for locating tumors targeted using magnetic nanoparticles, J. Nanobiotechnol. 13 (2015) 11.
[16] C. Johnson, N.L. Adolphi, K.L. Butler, M.L. Debbie, R. Larson, P.D. Schwindt, E.R. Flynn, Magnetic relaxometry with an atomic magnetometer and SQUID sensors on targeted cancer cells, J. Magn. Magn. Mater. 324 (2012) 2613–2619.
[17] F. Wiekhorst, U. Steinhoff, D. Eberbeck, L. Trahms, Magnetorelaxometry assisting biomedical applications of magnetic nanoparticles, Pharm. Res. 29 (2012) 1189–1202.
[18] J. Dieckhoff, D. Eberbeck, M. Schilling, F. Ludwig, Magnetic-field dependence of Brownian and Néel relaxation times, J. Appl. Phys. 119 (2016) 043903.
[19] D. Eberbeck, F. Wiekhorst, U. Steinhoff, L. Trahms, Aggregation behaviour of magnetic nanoparticle suspensions investigated by magnetorelaxometry, J. Phys.: Condens. Matter 18 (2006) S2829.
[20] J. Leliaert, D. Eberbeck, M. Liebl, A. Coene, U. Steinhoff, F. Wiekhorst, B. Van Waeyenberge, L. Dupré, The complementarity and similarity of magnetorelaxometry and thermal magnetic noise spectroscopy for magnetic nanoparticle characterization, J. Phys. D Appl. Phys. 50 (2017) 085004.
[21] O. Laslett, S. Ruta, J. Barker, R. Chantrell, G. Friedman, O. Hovorka, Interaction effects enhancing magnetic particle detection based on magneto-relaxometry, Appl. Phys. Lett. 106 (2015) 012407.
[22] W. Weitschies, R. Kötitz, L. Trahms, T. Bunte, Process and compounds for use in detecting analytes by measurement of residual magnetism, and the use of the said compounds, Google Patents (2006).
[23] R. Kotitz, H. Matz, L. Trahms, H. Koch, W. Weitschies, T. Rheinlander, W. Semmler, T. Bunte, SQUID based remanence measurements for immunoassays, IEEE Trans. Appl. Supercond. 7 (1997) 3678–3681.
[24] H. Matz, D. Drung, S. Hartwig, H. Groß, R. Kötitz, W. Müller, A. Vass, W. Weitschies, L. Trahms, A SQUID measurement system for immunoassays, Appl. Supercond. 6 (1999) 577–583.
[25] D. Eberbeck, C. Bergemann, F. Wiekhorst, U. Steinhoff, L. Trahms, Quantification of specific bindings of biomolecules by magnetorelaxometry, J. Nanobiotechnol. 6 (2008) 4.
[26] D. Eberbeck, C. Bergemann, S. Hartwig, U. Steinhoff, L. Trahms, Binding kinetics of magnetic nanoparticles on latex beads and yeast cells studied by magnetorelaxometry, J. Magn. Magn. Mater. 289 (2005) 435–438.
[27] F. Wiekhorst, M. Liebl, U. Steinhoff, L. Trahms, S. Lyer, S. Dürr, C. Alexiou, Magnetorelaxometry for in-vivo quantification of magnetic nanoparticle distributions after magnetic drug targeting in a rabbit carcinoma model, Magnetic Particle Imaging, Springer, 2012, pp. 301–305.
[28] F. Ludwig, S. Mäuselein, E. Heim, M. Schilling, Magnetorelaxometry of magnetic nanoparticles in magnetically unshielded environment utilizing a differential fluxgate arrangement, Rev. Sci. Instrum. 76 (2005) 106102.
[29] A. Haller, S. Hartwig, H. Matz, J. Lange, T. Rheinländer, R. Kötitz, W. Weitschies, L. Trahms, Magnetic nanoparticle relaxation measured by a low-Tc SQUID system, Supercond. Sci. Technol. 12 (1999) 956.
[30] J. Schambach, L. Warzemann, P. Weber, R. Kotitz, W. Weitschies, SQUID gradiometer measurement system for magnetorelaxometry in a disturbed environment, IEEE Trans. Appl. Supercond. 9 (1999) 3527–3530.
[31] E. Flynn, H. Bryant, A biomagnetic system for in vivo cancer imaging, Phys. Med. Biol. 50 (2005) 1273.
[32] S. Knappe, T.H. Sander, O. Kosch, F. Wiekhorst, J. Kitching, L. Trahms, Cross-validation of microfabricated atomic magnetometers with superconducting quantum interference devices for biomagnetic applications, Appl. Phys. Lett. 97 (2010) 133703.
[33] M. Batie, S. Bitant, J.F. Strasburger, V. Shah, O. Alem, R.T. Wakai, Detection of fetal arrhythmia using optically-pumped magnetometers, JACC. Clinical electrophysiology 4 (2018) 284.
[34] V.K. Shah, R.T. Wakai, A compact, high performance atomic magnetometer for biomedical applications, Phys. Med. Biol. 58 (2013) 8153–8161.
[35] E. Boto, S.S. Meyer, V. Shah, O. Alem, S. Knappe, P. Kruger, T.M. Fromhold, M. Lim, P.M. Glover, P.G. Morris, A new generation of magnetoencephalography: room temperature measurements using optically-pumped magnetometers, Neuroimage 149 (2017) 404–414.
[36] A. Borna, T.R. Carter, J.D. Goldberg, A.P. Colombo, Y.-Y. Jau, C. Berry, J. McKay, J. Stephen, M. Weisend, P.D. Schwindt, A 20-channel magnetoencephalography system based on optically pumped magnetometers, Phys. Med. Biol. 62 (2017) 8909.
[37] Y.M. Wang, X. Cao, G.H. Liu, R.Y. Hong, Y.M. Chen, X.F. Chen, H.Z. Li, B. Xu, D.G. Wei, Synthesis of Fe3O4 magnetic fluid used for magnetic resonance imaging and hyperthermia, J. Magn. Magn. Mater. 323 (2011) 2953–2959.
[38] J.F.D.F. Araujo, M.C. Costa, S.R.W. Louro, A.C. Bruno, A portable Hall magnetometer probe for characterization of magnetic iron oxide nanoparticles, J. Magn. Magn. Mater. 426 (2017) 159–162.
[39] L. Néel, Some theoretical aspects of rock-magnetism, Adv. Phys. 4 (1955) 191–243.